Dev Biol. Author manuscript; available in PMC 2024 April 26.

Published in final edited form as:
Dev Biol. 2024 April 01; 508: 107–122. doi:10.1016/j.ydbio.2024.01.008.

Distinct developmental patterns in *Anopheles stephensi* organ systems

Khushboo Agrawal[#a,c], **Sunil Prabhakar**[#b], **Baskar Bakthavachalu**[a,e,**], **Dhananjay Chaturvedi**[d,f,*]

[a]Tata Institute for Genetics and Society Centre at inStem, Bellary Road, Bangalore, 560065, India

[b]Centre for Cellular and Molecular Platforms, Bellary Road, Bangalore, 560065, India

[c]School of Biotechnology, Amrita University, Kollam, 690525, Kerala, India

[d]National Centre for Biological Sciences, TIFR, Bangalore, 560065, India

[e]School of Basic Sciences, Indian Institute of Technology, Mandi, 175005, India

[f]CSIR − Centre for Cellular and Molecular Biology, Hyderabad, 500007, India

[#] These authors contributed equally to this work.

Abstract

Anatomical profiles of insects inform vector biology, comparative development and evolutionary studies with applications in forensics, agriculture and disease control. This study presents a comprehensive, high-resolution developmental profile of *Anopheles stephensi*, encompassing larval, pupal, and adult stages, obtained through microCT scanning. The results indicate *in situ* anatomical changes in most organ systems, including the central nervous system, eyes, musculature, alimentary canal, salivary glands, and ovaries, among other organ systems, except for the developing heart. We find significant differences in the mosquito gut, body-wall, and flight muscle development during metamorphosis from other dipterans like Drosophila. Specifically, indirect flight muscle specification and growth can be traced back at least to the 4th instar *A. stephensi* larvae, as opposed to post-puparial development in other Dipterans like *Drosophila* and *Calliphora*. Further, while *Drosophila* larval body-wall muscles and gut undergo histolysis, changes to these organs during mosquito metamorphosis are less pronounced. These observations, and raw data therein may serve as a reference for studies on the development and the genetics of mosquitoes. Overall, the detailed developmental profile of *A. stephensi* presented here illuminates the unique anatomy and developmental processes of *Culicidae*, with important implications for vector biology, disease control, and comparative evolutionary studies.

[*] Corresponding author. CSIR-Centre for Cellular and Molecular Biology, Hyderabad, 500007, India. [**] Corresponding author. School of Basic Sciences, Indian Insitute of Technology, Mandi, 175005, India. baskar@iitmandi.ac.in (B. Bakthavachalu), dhananjay@ccmb.res.in (D. Chaturvedi).

CRediT authorship contribution statement

Khushboo Agrawal: Data curation, Investigation, Writing − review; & editing. **Sunil Prabhakar:** Conceptualization, Data curation, Formal analysis, Investigation, Methodology, Visualization, Writing − review; & editing. **Baskar Bakthavachalu:** Funding acquisition, Resources, Software, Supervision, Writing − review; & editing. **Dhananjay Chaturvedi:** Conceptualization, Data curation, Formal analysis, Funding acquisition, Investigation, Methodology, Project administration, Resources, Supervision, Validation, Visualization, Writing − original draft, Writing − review; & editing.

Europe PMC Funders Author Manuscripts

Europe PMC Funders Author Manuscripts

1 Introduction

Of the family *Culicidae*, over three thousand mosquito species inhabit various geographic and climatic habitats worldwide (Crans, 2004; Ramasamy and Surendran, 2016), functioning in their ecological niches. A fraction of these species acts as vectors for protozoan, filarial and viral pathogens, which cause infections in humans and consequent suffering. *Anopheles* mosquitoes are vectors for the malaria causing pathogen, *Plasmodium*. Between the years 2000 and 2020, 896,000 to 627,000 people succumbed to malaria yearly (Organisation WH, 2021). Though strategies to control the number of malaria cases have shown results over the years, the emergence of drug-resistant *Plasmodium* strains and insecticide-resistant vectors necessitate deploying other strategies focusing on the *Anopheles* mosquito (Huijben and Paaijmans, 2018). In addition, mosquitoes provide an alternate reference for studying insect biology (Matthews et al., 2020). A clear understanding of mosquito developmental processes may help gain insights into the evolution of insects and the mechanisms underlying their physiological processes and to develop new strategies for controlling insect pests and developing new insect-based products.

Mosquito anatomy, especially larvae and adults, has been extensively documented over the past century (Snodgrass, 1959; Harbarch and Knight, 1980). The advent of genome editing techniques and gene drive technologies have allowed for genetic studies in mosquitoes along the lines of *Drosophila* (Dong et al., 2022). *Drosophila* growth and development have been investigated in depth to understand the principles of tissue specification, signalling, remodeling and growth in larval, pupal and adult stages in molecular detail. Variations of these principles operate in the development of many species. These variations and their diverse outcomes are particularly notable across the insect world (Truman and Riddiford, 2019). Dipterans such as *Drosophila* and *Culicidae* which underwent divergence approximately 260 million years ago, are classified as holometabolous insects, with metamorphosis being the key step in their life cycle (Grimaldi and Engel, 2005). Genetic studies in *Drosophila* have provided a wealth of understanding in the field of developmental biology, including the identification of key developmental genes and pathways, the regulation of tissue differentiation and remodeling, and the molecular mechanisms underlying morphological changes. However, the lack of appropriate quantitative tools to assess anatomy has hindered the acquisition of comparable knowledge for organisms such as mosquitoes. In this study, we have utilized microCT scanning to meticulously document the anatomical features of *A. stephensi* mosquito through their late larva (4th instar), pupa, and adult stages of development.

From these sub-micron resolution scans, we have focused on the development of organ systems or tissue groups that are essential for behaviours that contribute to making mosquitoes efficient disease vectors. These tissues include the central nervous system, the alimentary canal, salivary glands, flight muscles, swim muscles and eyes. We find marked distinctions in the development of some of these tissues compared to *Drosophila*. In *Drosophila*, larval body wall muscles, midgut and salivary glands histolyse during metamorphosis (Denton et al., 2009; Farkas and Mechler, 2000; Bate et al., 1991). The central nervous system undergoes notable morphological changes and heavy cell-death-

dependent remodeling (Tissot and Stocker, 2000). *Drosophila* eye development is initiated after pupa formation from a post-embryonically specified imaginal disc (Baker et al., 2014). Indirect flight muscles that power adult wing beats, start developing post-pupariation. A subset of indirect flight muscles called dorsal longitudinal muscles, arise from the remnants of thoracic body wall muscles that escape histolysis and larval myoblasts that fuse to them (Fernandes et al., 1991a, 1996a).

As the data in this study shows, *Anopheles stephensi* development differs from *Drosophila* in the chronology of specific organ development while others stay similar. For instance, dorsal longitudinal muscle (DLM) primordia in *Anopheles* are detectable in fourth instar larvae whereas remnants of *Drosophila* larval syncytia take on the role of dorsal longitudinal muscle templates only post pupariation. External *Drosophila* ommatidia emerge during the mid-pupal stage within the pupa whereas *Anopheles* ommatidia structurally mature at a comparable stage. However, both *Drosophila* and *Anopheles* salivary glands are undetectable at some point in the pupal stage. We further make such comparisons in detail in the following.

The findings, raw data, data collection and analysis methods presented in this study may serve as a map or frame of reference to explore *Anopheles* development in cytological and molecular detail.

2 Results

2.1 High-resolution whole animal imaging of Anopheles stephensi using microCT scanning

As with all *Culicidae, A. stephensi* larvae and pupae are obligate still-or slow-moving-water dwellers while adults need to feed on land while laying eggs in water under constant predatory pressure at all stages. They require an aqueous environments as eggs, four subsequent larval instar stages, and pupae. Adults eclosing from these pupae rely on terrestrial plants and animals for sustenance (Nikbakhtzadeh et al., 2016). The female mosquitoes' blood diet enables them to act as vectors for the transmission of the malarial parasite *Plasmodium falciparum*. The duration of the offspring's emergence, offspring size and survival depend on the resource availability and the environment in which they develop (Grech et al., 2007). *Culicidae* morphology and anatomy has adapted to each of these environments. The degree and sources of such selections, among them probable predatory pressures from both aquatic and terrestrial niches, may be responsible for stage specific form and function of varying organ system development, some of which we report in this study.

The necessity of stage specific form and function of different organ systems may contribute differences in developmental processes from purely land-dwelling insects such as *Drosophila*. These variations that include: photosensitivity of even the larval rudiments of the compound eye (Seldin et al., 1972); large larval and pupal abdominal swim muscles for rapid movement in water supported by abdominal innervation and their swift disappearance in adults when they may impede flight; differences in gastrointestinal structure to digest diets entirely different from adults; the lack of requirement of salivary glands when the animals do not feed (as pupae); indirect flight muscle development initiation before

relatively short pupal stage to expedite flight in freshly eclosed adults; sexual dimorphism as in the case of eyes of adults, probably arise owing to differences in diet and risks involved in obtaining it. In each case, predatory pressures in both aquatic and terrestrial environments may have dictated the divergence of individual organ system's developmental timelines from insects living exclusively in one or the other niche.

With the aim of outlining morphological and anatomical changes in *Anopheles*, especially in the pupal stage about which literature is scant, we raised *A. stephensi* under standard laboratory conditions as described in the methods section (Fig. 1). Within the limits of our method and instrumentation, clear discernible structures were obtained from 4th instar larvae and later developmental stages. Representative samples of these stages were studied, analyzed and presented using microCT scanning (Metscher, 2009a; Schoborg, 2020).

Broadly, fixed, heat-inactivated samples of appropriate stage were submerged in Iodine solution for the appropriate time as described in the methods section. Suitably mounted single or multiple samples were scanned under standardized conditions. Reconstruction, annotation, analysis and volume rendering steps that follow are all done *in silico* (Fig. 1). Fig. S1 shows unannotated sagittal plane views through early 4th instar larval, 48hr pupal and blood fed adult-female reconstructions to illustrate the detail provided by reconstructed images. Eight abdominal segments seen consistently in larvae, pupae and adults have been previously annotated (Jarvela et al., 2020; Clements, 1999). Posterior to the abdominal segment VIII, two terminal segments clearly seen in larvae are the siphon and anal segment (FOSTER and WALKER, 2002).

In this manner, we have assembled a picture of the development of indirect flight muscles, the gastrointestinal tract, compound eyes, salivary glands, central nervous system, ovaries and swim muscles in *A. stephensi*. Identification of these organs is based on accepted works (Snodgrass, 1959; Clements, 1999) and comparison with known structures in *Drosophila*. In pupae, these structures are identified based on their position and shape relative to larval and adult structures. The data presented lay the map for a more rigorous molecular assessment of these organs.

2.2 A. stephensi indirect flight muscle positioning and growth between 4th instar larval and adult stages

Indirect flight muscles power wing-beating in insects. *Culicidae* depend on the functioning of these muscles for locomotion towards food and habitation and away from predators. These muscles occupy a large proportion of the thoracic cavity. They are further grouped into Dorsal Longitudinal Muscles (DLMs) and Dorso-Ventral Muscles (DVMs) based on their body-wall attachment points. Dorsal longitudinal muscles are positioned in the anterior-posterior direction while dorso-ventral muscles are somewhat orthogonal to them (Deora et al., 2017). Their asynchronous contraction and relaxation cycles allow the *Anopheline* mosquito wing beat frequency to reach 320-770 Hz (Caprio et al., 2001; OGAWA and KANDA, 1986). A new approach for vector control involves genetic tools that specifically target the development of indirect flight muscles in female mosquitoes, with the aim of blocking their flight capabilities (Fu et al., 2010).

The stereotypical positioning of DLMs in adults results from an intriguing developmental process that is well characterized in *Drosophila* (Fernandes et al., 1996; Fernandes and Keshishian, 1996). After transitioning past 3rd instar into a pupa, larval body wall muscles are lost through histolysis. Specific syncytia in the T2 segment, a remnant from larval body wall muscles, escape histolysis after pupariation. Subsequently, myoblasts from an embryonically specified lineage fuse with these syncytia. Consequently, these to-be dorsal longitudinal muscles grow to the shape and position seen in wild-type animals. Dorso ventral muscles rely solely on myoblasts for their specification and growth without the intervening step of fusing with remnants of body wall syncytia. Even so, their formation starts after pupariation (Bothe and Baylies, 2016).

As seen from microCT scans of adult *A. stephensi*, DLMs and DVMs retain their positioning within the thorax (Fig. 2H-K). Distinct from *Drosophila*, dorsal longitudinal muscles and dorsoventral muscles in each thoracic hemi segment consist of three muscle bundles, each subdivided into four fibers. The same structures were marked out in younger stages of development (0-2hr pupa (early), 24hr, 48hr (late)) (Fig. 2E-G). They appear closer to the thorax wall at younger stages (Fig. 2C and D insets). Intriguingly though smaller in volume at the onset of pupariation, DLMs and DVMs retain their relative positions, bundle numbers and constituting fibers. Smaller structures with the same relative position, bundle and fiber numbers are clearly visible in the late 4th instar larvae (Fig. 2C and D). Notably, structures similar to DVMs cannot be detected from our CT scans of early 4th instar larvae (Fig. 2A and B). Employing cellular lineage tracing and genetics tools to ascertain if DVM formation occurs through founder cells as in *Drosophila* without templates would be very informative.

These observations were unexpected and quite remarkable given their departure from the developmental timeline of a model system such as *Drosophila*. The expression pattern of indirect flight muscle-specific *Act4* gene along with recent histological analyses in *Aedes* 4th instar larvae, support our conclusions regarding larval *Anopheles* indirect flight muscle precursors based purely on CT scans (Fu et al., 2010; Celestino-Montes et al., 2021).

2.3 A. stephensi swim muscle positioning between 4th instar larval and adult stages

Anopheles larvae and pupae move in their aquatic habitat using power strokes generated from the swim muscles. By segmenting microCT reconstructions based on voxel intensity and size thresholding and continuity, with considerable refinement using the methods outlined in our study, we were able to identify a regular pattern of abdominal muscles that are responsible for this movement (Fig. 3). They primarily occupy the dorsal and ventral sides within the abdomen. Notably, with our segmentation protocol, this group of muscles can be seen extending into the thorax in larvae and pupae (Fig. 3A-C insets), suggesting they may also contribute to swimming function at these stages of mosquito development. Surprisingly, these muscle structures are visible even in freshly eclosed adults (Fig. 3D). It appears that the histolysis of larval swim muscles is completed between Day 0 and Day 5 post-eclosion as they are not detected in 5-day old post-eclosion (p.e.). adults. Incomplete histolysis in 2-Day p.e. adults have been previously reported (King and Hillyer, 2013).

2.4 Changes to A. stephensi central nervous system between 4th instar larval and adult stages

The Adult *Anopheles* central nervous system consists of the brain and ventral nerve cord (VNC) extending into the thoracic ganglia further innervating the abdomen via the abdominal ganglia (Brown and Cao, 2001). In our segmentation of these structures (Fig. 4) starting with 4th instar larvae, we find they are positioned similarly at all developmental stages analyzed (Fig. 4A-F insets). It must be noted that these scans do not distinguish finer innervation, cellular arrangements and activity. The brain and Sub Oesophageal Ganglia (SOG) are contained within the head. Three contiguous thoracic ganglia can be seen within the thoracic segment. The nervous system further extends from there into the abdomen with at least one ganglion per segment, barring the terminal two segments (Fig. 4A-F).

A detailed depiction of the development of the thoracic and abdominal neuropil is shown in Fig. 5. Two prongs of the descending ventral chord connect to thoracic ganglia, with T1, T2, and T3 being very distinct in larvae but they bundle close together in pupae and adults (Fig. 5A-C). In larvae, abdominal ganglia can be seen at the anterior ventral midline of each segment, with a total of eight ganglia being most frequently counted at the start of the 4th instar based on the volume (Fig. 5D). The total volume of the abdominal neuropil does not significantly change up until 48hr pupal stage (Fig. 5E). The volume of the thoracic neuropil increases between 4th instar larvae and 24hr pupae and stabilizes thereafter (Fig. 5F). At two subsequent stages, the abdominal neuropil shrinks successively, and the number of abdominal ganglia most frequently goes down to six in adults (Fig. 5G). Larval A1 is undetectable in adult scans based on position, and larval A7 and A8 appear to have fused in adults (Supplementary Materials: Tables 1-3). The exact cellular changes and mechanisms behind such remodeling during the development of the thoracic and abdominal neuropil may help in understanding any functional alterations.

2.5 A. stephensi alimentary canal and salivary gland positioning and growth between 4th instar larval and adult stages

The digestive system, including the alimentary canal and associated salivary gland, is not only key to the survival of most organisms, but in the case of *Anopheles*, crucial organs for the *Plasmodium* parasite life cycle and malaria spread in human populations. *Plasmodium* sporozoites emerge from oocysts in the midgut wall and circulate in the hemolymph before invading salivary glands, which serve as repositories for sporozoites that get injected into a vertebrate host during a blood meal. Therefore, establishing a clear morphological baseline during the developmental process of these organs is essential to assess the effects of both harboring parasites and for implementing strategies to control their spread.

The alimentary canal of *A. stephensi* yielded by our segmentation protocol clearly shows the distinct anatomy of the gut in early 4th instar larvae and in adults. In early 4th instar larvae, gastric cecae are prominent compartments contained within the thorax, extruding at the anterior of midgut, which is much wider extending to the 5th abdominal segment (Fig. 6A). In late 4th instar larvae, segmented gastric cecae appear reduced in size (Fig. 6B). Shortly after pupariation, the signal of the gut is not as clear with our segmentation protocol, suggesting remodeling of this tissue (Fig. 6C). A ceca-like protuberance can be seen

associated with the alimentary canal halfway through pupariation (Fig. 6D), but not prior to eclosion (Fig. 6E). The adult alimentary canal (Fig. 6F) appears significantly different in structure relative to the larval one. Notably, our segmentation protocol has not yielded the dorsal diverticulum and crop expected to be seen at the anterior end of the midgut or the malphigian tubules at its end (Novak et al., 1995). Further, our gut segmentation output includes the gonads from larval and pupal stages, though a separate segmentation has been developed for ovaries (Result section 2.6, Fig. 8).

The salivary glands are located in the mosquito thorax flanking the oesophagus. Based on previously illustrated positions (Novak et al., 1995; James and Rossignol, 1991), these structures were annotated manually on reconstructed data (Fig. 6). At this resolution, we can mark the glands without distinguishing the lateral and median lobes. Salivary glands could be discerned from our scans in 4th instar larvae (Fig. 7A and B) and adults (Fig. 7C and D) but not in pupae. The combination of data resolution and pupal salivary gland histolysis is likely contributing to this observation (Rishikesh, 1959; Chiu et al., 2021).

2.6 Positioning and growth of ovaries between 4th instar larval and adult stages in A. stephensi

As in *Drosophila, Anopheles stephensi* ovary development is initiated prior to pupariation. In our datasets, the anterior ends of ovaries are consistently located in the sixth abdominal segment. Their posterior ends extend into the anterior seventh abdominal segment of 4th instar larvae (Fig. 8A-B). Average ovary volumes increase by nearly seventy percent between early and late 4th instar larval stages (Fig. 8K). Our segmentation detects lateral oviducts extending further into the seventh abdominal segment of 0 h pupae (Fig. 8C). Over the next 24 h though volumes appear not be statistically different, the increase in surface area of ovaries suggests elongation of ovariole like structures (Fig. 8D, J, K). Histological analysis may confirm this conjecture.

By 48 h post pupa formation overall ovary volumes increase significantly and clearly defined lateral oviducts can be segmented, probably meeting in the common oviduct in the eighth abdominal segment. In freshly eclosed adults, the anterior end of ovaries can now be seen approaching the fifth abdominal segment with clearly defined ovarioles (Fig. 8F). The increase in surface area in this duration without concomitant increase in volumes may be a result of this development (Fig. 8J and K). A marked increase in oogenesis contributes to a near threefold increase in both average volume and surface area as females complete 5 days of adulthood (Fig. 8J and K). In this window, the anterior end of ovaries that bear germaria are no longer limited to the sixth abdominal segment, suggesting that any adhesion of germaria to the body wall may have been relieved (Fig. 8f). Without a bloodmeal, ovary volumes do not significantly change between day 5 and 10 of eclosion, though the average volumes have gone up approximately five (4.87) times since pupariation. However, females given a bloodmeal at five days post eclosion show over a forty (42.6) fold increase volume at 14 days post eclosion relative to unfed 10 day old females.

2.7 A. stephensi eye positioning and growth between 4th instar larval and adult stages

Owing to aquatic and terrestrial niches, larval and adult mosquito eyes contend with media of different refractive indices. Yet, individuals in both developmental stages respond to light, albeit in different ways (Hawkes et al., 2017; Thomas, 1950; Kawada et al., 2006). Underlying structural changes to developing eyes and brains may be responsible for these differences. Early *Aedes* larval eye development, starting with optic placode formation in the first instar has been described (White, 1961). The basic unit of a compound insect eye is called an ommatidium. An ommatidium unit is comprised of a rhabdom positioned below a near hemispherical corneal lens facet. As found in several mosquito species, the rhabdom shape approximated to an inverted cone with its tip abutting the planar surface of the facet.

Our scans allow us to assess changes during *A. stephensi* eye development in detail. The development of insect compound eyes (stemmata) is intriguing (Rocha et al., 2015). In *Anopheles*, fields of developing ommatidia remain separated up to at least the onset of pupariation (Fig. 9A-C). From our scans, we see adult *Anopheles* compound eyes have arrays of ommatidia laid over the lateral portion of the head, and joint at the ventral midline (Fig. 9G, inset). This joint appearance can be seen as early as 24hr pupae (Fig. 9D-F). The ordered appearance of adult ommatidia allows us to set threshold parameters to segment for mature ommatidia appearance during development. As can be seen in Fig. 10A-D, developing ommatidia range in shape between larval and 24hr pupal stages. More defined shapes and arrangement of ommatidia are apparent from 24hr pupal to adult stages.

We utilized volume and surface area data from combined male and female scans to determine when the ommatidia in *Anopheles* eyes develop in-depth as opposed to spread. The volumes of eye structures increase rapidly during pupal stages and eclosion and then stabilize (Fig. 10G), while the increase in the surface area appears to occur between the onset of pupariation and 24hrs thereafter, which does not change significantly afterward (Fig. 10H). Because *Anopheles*'s eyes at this stage resemble a truncated curved cone, we assessed the onset of an increase in depth by measuring the individual ratios of volume to the surface area. This one-dimensional ratio is directly proportional to the change in depth. The distribution of these ratios changes significantly between 24 and 48hr pupal stages, indicating that the largest increase in ommatidial depth occurs during these stages (Fig. 10I). Changes before and after these stages are statistically not significant.

A notable difference between adult male and female *Anopheles* eyes includes differences in the total surface area and mature ommatidia number and diameters (Fig. 10J-L). Surface areas of the female eye significantly exceed those of males (Fig. 10J). This difference may be attributed to both increased numbers of ommatidia (Fig. 10K) and a small but statistically significant increase in dimensions of ommatidia (Fig. 10L) (Supplementary Materials: Tables 4-9). The same geometric definition of ommatidia is used across all scans, which may account for the bimodal appearance of volume and surface area distribution at all developmental stages (Fig. 10G-I). Differences in ommatidia numbers have been previously noted in *Drosophila* (Surkova et al., 2021), and larger ommatidia have been reported in female band-wing grasshoppers (Duncan et al., 2021). Understanding the developmental origins of these sexual dimorphisms under the same developmental program can help

compare fitness differences between males and females, after normalizing for habitat, predator pressure, food availability, and modes of derivation.

These observations serve as a timeline for a more detailed study inspecting the underlying molecular changes, if any, to cellular structure and innervation of developing eyes as they transit from aquatic to terrestrial niches.

3 Discussion

The study of mosquito anatomy has been of great interest for several decades (Snodgrass, 1959). Anatomical studies in mosquitoes were limited to light and electron microscopy to observe the detailed structures at different scales. Most internal anatomy requires tissue dissection which creates artifacts or fails to provide quantitative data in the native architecture. This becomes more challenging for the remodeling stages of development such as insect metamorphosis, most rapid in pupal stages.

Understanding mosquito anatomy is crucial to understand its biology and behavior as well as to developing new vector control strategies and traps that can specifically target certain mosquito species based on their physical characteristics (Hill and Ignell, 2021). Having a detailed anatomical reference map of mosquitoes will help compare and study the effects of chemical, microbial, or genetic manipulations currently being developed for vector control.

Non-invasive imaging techniques such as microCT have been useful in revealing anatomy without the need for dissection (Metscher, 2009b; Schoborg et al., 2019; Hall and Martín-Vega, 2019). Mosquito species are of particular interest and various imaging techniques, such as Optical coherence tomography, Optical Projection Tomography, Light Sheet Fluorescence Tomography and X-Ray based imaging through TOMCAT have been attempted to visualize them *in situ* (Ravichandran et al., 2017; Muijres et al., 2017; Niz et al., 2020).

We present a detailed anatomical map of *A. stephensi* across its development from late larval to adult stages. The data presented include a comparison of different organ development and a comprehensive analysis tool. Though the study focuses on specific organs, full-resolution reconstructed datasets are available to anyone for further examination.

We show *in situ* positioning of organs critical to *Anopheles* survival and hosting *Plasmodia* at sub-micron resolution from post-3rd instar larval stages of development. Indirect flight muscles in insects have been extensively studied due to their fundamental importance in insect flight. The anatomy, physiology, and biomechanics of indirect flight muscles have been the subject of numerous investigations across various insect species. We find that though the positioning of indirect flight muscles is similar to *Drosophila*, the muscle fiber numbers and organization as well as timelines of development in relation to pupariation differ between *Anopheles* and *Drosophila*. These observations pose several interesting questions; a) Does thoracic musculature in 1st -3rd instar *Anopheles* histolyse leaving behind escaper syncytia that are to be indirect flight muscle precursors? b) Do *Anopheles* DVMs develop from the fusion of myoblasts to founder cells through molecular mechanisms similar to *Drosophila*?

Europe PMC Funders Author Manuscripts

The clear anatomical documentation has implications that extend into purely functional studies as well. For instance, how does extensive alteration to abdominal muscles post eclosion, or the change in flight muscle fiber number and arrangement relative to other dipterans factor into the mathematical characterization of flight biomechanics?

The evolution of species' forms decides function and therefore fitness. Some variants of molecular pathways governing the development of specific organ systems may be favored over others. For instance, within subgroups of muscles, molecular pathways governing flight muscles and abdominal muscles in *Drosophila* are keenly characterized relative to mosquitoes. Both muscle subgroups contribute distinct advantages in the native environments of these dipteran insect species.

Mosquito larvae and pupae are under predatory pressure from fish, frogs and insects in a variety of habitats (Louca et al., 2009; Medlock and Snow, 2008; Baldwin et al., 1955). Motility is likely a key parameter in mosquito larvae and pupae evading predation, as it is in other species (Lindstedt et al., 2019). Compared to larvae, Aedes pupae cover smaller distances under laboratory conditions, thus probably elevating pupal predation risk, even in the wild (Tomé et al., 2014). It is therefore conceivable that molecular mechanisms promoting motility at all stages of *Anopheles* development are weighted for selection within these environments. These mechanisms would include the late disappearance of abdominal swim muscles post eclosion and early onset of flight muscle development relative to *Drosophila* (VijayRaghavan et al., 1991; Fernandes et al., 1991b, 1996; Zirin et al., 2013), as we report here.

Furthermore, understanding the anatomy of the mosquito's nervous system can inform the development of control methods that interfere with the mosquito's ability to fly or transmit disease. The mosquito nervous system is of great interest to several labs around the globe interested in understanding how mosquitoes detect and respond to various stimuli, such as odors, heat, and visual cues, which are crucial for their host-seeking and blood-feeding behaviors (Hill and Ignell, 2021). In addition, studying the mosquito nervous system can provide insights into basic neuroscience questions, such as the organization and function of neural circuits that control behavior.

The nervous system of *A. stephensi* appears to retain its layout: the brain, ventral nerve cord and thoracic ganglia are positioned in the head and thorax, with clearly defined abdominal ganglia at each abdominal segment can be seen right from the 4th instar to adult stages. How, and by how much, the cell numbers, cell identities and circuits change and mature, in this organ system changing anatomy, would be interesting to ascertain. However, the data did not allow for distinguishing finer innervation, cellular arrangements, and activity. Our observations and method may contribute to systematic studies of insect central nervous system evolution as reviewed in Niven et al. (2008).

The anatomy of mosquitoes, particularly their digestive system and associated salivary glands, plays a crucial role in the transmission of malaria to humans. The *Plasmodium* parasite relies on the midgut and salivary glands of *Anopheles* mosquitoes to complete its insect life cycle and spread to human hosts. Therefore, it is essential to have a clear

understanding of the morphological development of these organs in order to implement effective disease control strategies. Attempts are being made to express anti-malaria antibodies in mosquito midgut to block parasite lifecycle using genetic engineering approaches (Keleta et al., 2021). We believe our segmentation protocols have yielded important insights into the distinct anatomy of the gut in early and late 4th instar larvae and in adults. Furthermore, the location and appearance of the salivary glands in 4th instar larvae and adults have been annotated manually on reconstructed data, providing valuable information for future research (Truman and Riddiford, 2019)

It is likely that methods of anatomical documentation as employed in this study, coupled with data about the fitness of the species in its ecological niche will provide clearer insights about selective pressures on development. Interesting comparative physiology questions that build towards such an understanding include, how do endocrine mechanisms, such as Juvenile hormone and ecdysone signaling, that govern muscle development and histolysis differ between insect species e.g. How is *Anopheles* indirect flight muscle specification and development induced prior to pupariation? How do mosquito swim muscles escape histolysis? Are the mechanisms governing the escape of histolysis of DLM templates in *Drosophila* and swim muscles in mosquitos conserved or merely convergent?

Recent findings in inter-organ communication observed in other dipterans (Malita and Rewitz, 2021; Ahmed et al., 2020; Meschi et al., 2019), motivate the concurrent measurement of anatomical changes in multiple organ systems in response to metabolic, genetic and environmental variations. The ability to record these changes non-invasively *in situ* with conventional light microscopy at desired scale and resolution has been a limiting factor. In the past decades of advances in X-ray based computer tomography and more readily available computing power has facilitated soft tissue visualization without invasive procedures (Metscher, 2009a, 2009b; Schoborg et al., 2019; Alba-Tercedor et al., 2021; Chaturvedi et al., 2019). Applications of these techniques may prove vital to studies of disease vectors, pests, or species key to the functioning of ecosystems. The powerful combination of detailed molecular analyses of model systems, with the ability to judiciously manipulate conserved mechanisms across an ever-growing list of newly documented insect species buttressed with accurate measurements of their effects, promises to be the basis of a clearer understanding of biology within individual organisms to ecosystems in general.

The current study documents different stages of *Anopheles*' development post 4th instar, because of the technical limitations. A complete anatomical map of *Anopheles* development with 3rd, 2nd, and 1st instar stages, and possibly embryo would employ similar tissue preparation but with higher resolution NanoCT scanning.

4 Materials and methods

4.1 Mosquito maintenance

Anopheles stephensi, mosquito colonies were reared and maintained at 27 °C ± 1 °C, 12:12 h light: dark diurnal cycle at 80 % relative humidity. A mixture of Yeast (Bluebonnet Nutrition, Brewer's yeast) and powdered Dog biscuits (Pedigree) in a 3:1 ratio was used to feed larvae. Adult mosquitoes were reared in cages with 10 % sucrose solution.

Europe PMC Funders Author Manuscripts

4.2 Synchronous egg laying

Four days old female mosquitoes were fed blood using a heamotek membrane feeding system. After 3 days of blood-feeding, 5–6 random gravid females were selected and transferred to plugged tubes containing moist cotton and lined with moist Whatman filter paper at the bottom.

The tubes were placed in a humid chamber at 28 °C protected from light for 30mins to facilitate oviposition. The resulting eggs were incubated in moist conditions for completion of embryonic development for 40-48 h. Post this, eggs were transferred to a plastic tray containing RO water. The water was changed every 2-3 days based on the turbidity levels. Larval food was added in small quantities to the tray every day.

4.3 Sample collection and preparation

Larvae—The day of hatching was considered day 0. Larval samples were collected every alternate day starting day 3. The collected larval samples were fixed in a microcentrifuge tube containing 4 % paraformaldehyde (PFA) in PBS, ensuring the sample was completely submerged. The samples were incubated at room temperature overnight with gentle shaking. Post this, the fixative was gently aspirated and discarded, followed by two washes with 1 ml PBS for 15 min at room temperature. Each tube was filled with 200 µl of staining solution containing 1 % elemental iodine (1.93900.0121, Emparta, Merck) and 2 % potassium iodide (no. 15,724, Qualigens) dissolved in PBS ensuring the specimens were submerged. The staining was carried out with gentle shaking at room temperature for 4-5 Days.

Pupa—Late 4th instar larvae were monitored hourly and the pupae formed in this interval were collected and considered as early pupae. Three different batches of these synchronous early pupae were collected, and two of these batches were allowed to age for 24 h (mid-age) or 48 h (Late) respectively.

All pupae at their respective time point were fixed in a micro-centrifuge tube containing 4 % PFA in PBS. The samples were heat inactivated by placing them in a 65 °C dry bath for 1-2 min. These samples were then incubated at room temperature overnight with gentle shaking. Post this fixative was aspirated out gently, followed by two 15-min washes with 1 mL of PBS per tube at room temperature. A 200 µl staining solution was added to the tubes making sure all pupae were submerged. Samples were incubated at room temperature with gentle shaking for 4-5 Days.

Adults—Late Pupae were separated and placed in cages. Mosquitoes that emerged within an hour were considered as 0-day adults. Similarly, synchronously collected adults were aged for 5 days and 10 days. 5-day old females were blood-fed with human O + ve blood obtained commercially from a blood bank using the Hemotek membrane feeding system.

At respective time points, adults were collected from the cages using a mouth aspirator in a plugged tube. Mosquitoes were anaesthetized on a carbon pad and males and females were separated. These mosquitoes were then fixed in PBS containing 4 % PFA and 0.2 % Triton X-100 (Sigma -Aldrich) in a microcentrifuge tube ensuring the specimens were submerged. These samples were then incubated at room temperature overnight with gentle mixing. Post

this fixative was aspirated out gently and discarded, and the samples were washed twice in 1 ml PBS for 15mins at room temperature. Next, 30-100 µl of staining solution was then added to the tubes making sure all adult mosquito samples were submerged. Samples were incubated in the staining solution at room temperature with gentle mixing for 4-5 Days.

	Larvae	Pupae	Adults
Fixing	4 % PFA in PBS, overnight at room temperature.	4 % PFA in PBS,1-2 min. Heat inactivation at 65 °C of Animal and then overnight at room temperature.	4 % PFA, 0.2 % Triton X-100 in PBS, overnight at room temperature.
Washes	3X 15 min PBS washes	3X 15 min PBS washes	3X 15 min PBS washes
Staining	4-5 days incubation in staining solution with gentle shaking at room temperature	4-5 days incubation in staining solution with gentle shaking at room temperature	4-5 days incubation in staining solution with gentle shaking at room temperature

4.4 MicroCT scanning of iodine stained mosquito samples

Prepared samples were coated with paraffin oil to prevent dehydration and iodine sublimation during scanning (Fig. 1B). Oil-coated prepared samples were mounted in petroleum jelly-filled polypropylene pipette tips of accommodating size. Single or multiple samples can be mounted in pipette tips at appropriate times to normalize scanning conditions and minimize the need for human intervention during the scanning process (Fig. 1C). Samples are mounted with their anterior-posterior axis as close to colinear with the stage's rotation axis as possible. All scans were performed on the Bruker SkyScan1272, 16Mp CCD camera, microCT scanner. All scans were 180° total rotation of the sample. 0.1°. 0.2° and 0.4° rotation step sizes that yielded 1880, 939, 470 raw images per scan of larvae, pupae and adults respectively. Scans were performed at 40 kV, 250 mA, 4940X3280 pixels, averaging set to 2, without filters at 0.8µ resolution. For samples that exceeded the field of view at this resolution, over-sized scanning was used: two overlapping scans were aligned and stitched in NRecon software.

4.5 Data preparation for analysis

Tomograms of the whole animals were generated from projection image stacks using the Bruker NRecon. A region of interest outlining the tissue reconstructed area was marked on the preview image. The range of the X-ray attenuation coefficient detected in the tomogram preview was applied to the rest of the reconstruction planes. Ring artifact reduction between 10 and 30 units was applied based on manual inspection of the tomogram preview. For single and multi-frame scans, NRecon-generated values were used for misalignment corrections. The reconstruction engine parsed through every plane of the specimen projection view applying frame-specific misalignment corrections and saved its tomogram as an indexed 8-bit PNG format image. The 3D reconstruction of the specimen finally comprised an image volume whose elements were voxels of isotropic size.

Prior to tissue segmentation, re-orientation of the reconstructed image volume was followed by its downsizing by a factor of 4 on all axes in Bruker DataViewer. On reoriented volumes with matching downsizing, segmented tissue was overlaid on the reference image volume as a target image. Manual corrections in alignment were performed where necessary. Post

alignment, thresholding for the background was performed using the Automatic Ridler-Calvard-2Dmethod. Voxel registration was performed in "pseudo-3D" automatic mode with an error margin of 50 pixels. Reconstructed stacks were binarized. The final step prior to extraction of dimensions, was further despeckling and removal of objects on the margin as well as disconnected tissue.

4.6 Analysis of individual organs

Dimensions for CNS, gut, salivary gland, indirect flight muscles, and swim muscles were extracted from the masks obtained by the above method in CTAN.

For eye facet counts, further processing of the segmented eyes was performed as follows. For pupal and adult stages of the insect life cycle, the compound eye outline was inclusive of the cornea and the underlying rhabdom layer. For the larval stage, the eye disc outline was traced from anterior to posterior parts of the head. The boundaries were readjusted manually to exclude the optic nerve tissue. The segmented image volume thus represented the entire eye tissue and was binarized using the routine below for doing morphometric measurements.

4.7 Eye facet counts

To segment facets, that we use to approximate ommatidia diameter, cross-sectional CT reconstructions of the adult *A. stephensi* eye revealed a bilayer of tissue. The layer surfacing the head cuticle was comprised of a lattice-structured cornea overarching the rhabdom layer. To enhance the contrast of edges separating these layers, anisotropic diffusion followed by Gaussian blurring was used. Corneas were further separated from the underlying layer by appropriate erosion. To count facets and measure their diameter, we fragmented this lattice sheet into corneal objects using the watershed separation method. Further counts were obtained in CTAN.

4.8 Statistics and plotting

Contiguous age groups were tested pairwise for statistical significance using Wilcoxon's rank-sum test (Matlab). Violin plots for tissue volume, surface area and average tissue [volume/surface area] depth of the sorted groups were generated using the Seaborn library imported into Matlab via a Python. Violin plots of neuropil volume for the sorted groups were generated for the thorax and abdomen segments separately using the Seaborn library. Additional adjustments to the dimensions of SVG outputs were made in Adobe Illustrator.

Supplementary Material

Refer to Web version on PubMed Central for supplementary material.

Acknowledgments

We thank Bangalore Life Science Cluster (BLiSC) EM facility for providing us access to their microCT instruments and offering their support. We would like to extend our appreciation to Dr. Sunita Swain (TIGS) and the entire insectary team at DBT-inStem and TIGS-CI for their extensive assistance. We are thankful to Dr. Suresh Subramani for his valuable comments on the manuscript. BB acknowledges the support received from the Tata Institute for Genetics and Society and the DBT/Wellcome Trust India Alliance Fellowship (IA/I/19/1/504286). We also acknowledge the DST INSPIRE fellowship awarded to KA and the logistical support provided by

C-CAMP. DC acknowledges the Campus Fellowship at NCBS and DBT/Wellcome Trust India Alliance Fellowship (IA/I/22/2/506508) for support.

Data availability

Data will be made available on request.

References

Ahmed SMH, Maldera JA, Krunic D, Paiva-Silva GO, Pénalva C, Teleman AA, et al. Fitness trade-offs incurred by ovary-to-gut steroid signaling in Drosophila. Nature. 2020; 584 (7821) 415–419. [PubMed: 32641829]

Alba-Tercedor J, Hunter WB, Alba-Alejandre I. Using micro-computed tomography to reveal the anatomy of adult Diaphorina citri Kuwayama (Insecta: Hemiptera, Liviidae) and how it pierces and feeds within a citrus leaf. Sci Rep-uk. 2021; 11 (1) 1358.

Baker NE, Li K, Quiquand M, Ruggiero R, Wang LH. Eye development. Methods. 2014; 68 (1) 252–259. [PubMed: 24784530]

Baldwin WF, James HG, Welch HE. A study of predators of mosquito larvae and pupae with a radio-active Tracer1. Can Entomol. 1955; 87 (8) 350–356.

Bate M, Rushton E, Currie DA. Cells with persistent twist expression are the embryonic precursors of adult muscles in Drosophila. 1991; 89: 79–89.

Bothe I, Baylies MK. Drosophila myogenesis. Curr Biol. 2016; CB 26 (17) R786–R791. DOI: 10.1016/j.cub.2016.07.062

Brown MR, Cao C. Distribution of Ovary Ecdysteroidogenic Hormone I in the nervous system and gut of mosquitoes. J Insect Sci. 2001; 1 (1) 3. [PubMed: 15455063]

Caprio MA, Huang JX, Faver MK, Moore A. Characterization of male and female wingbeat frequencies in the Anopheles quadrimaculatus complex in Mississippi. J Am Mosquito Contr. 2001; 17 (3) 186–189.

Celestino-Montes A, Hernández-Martínez S, Rodríguez MH, Cázares-Raga FE, Vázquez-Calzada C, Lagunes-GuilĺEn A, et al. Development of the indirect flight muscles of Aedes aegypti, a main arbovirus vector. BMC Dev Biol. 2021; 21 (1) 11. [PubMed: 34445959]

Chaturvedi D, Prabhakar S, Aggarwal A, Atreya KB, VijayRaghavan K. Adult Drosophila muscle morphometry through microCT reveals dynamics during ageing. Open Biol. 2019; 9 (6) 190087 [PubMed: 31238820]

Chiu M, Trigg B, Taracena M, Wells M. Diverse cellular morphologies during lumen maturation in Anopheles gambiae larval salivary glands. Insect Mol Biol. 2021; 30 (2) 210–230. [PubMed: 33305876]

Clements AN. The biology of mosquitoes. Sensory Reception and Behaviour. 1999; 2

Crans WJ. A classification system for mosquito life cycles: life cycle types for mosquitoes of the northeastern United States. J Vector Ecol J Soc Vector Ecol. 2004; 29 (1) 1–10.

Denton D, Shravage B, Simin R, Mills K, Berry DL, Baehrecke EH, et al. Autophagy, not apoptosis, is essential for midgut cell death in Drosophila. Curr Biol. 2009; 19 (20) 1741–1746. [PubMed: 19818615]

Deora T, Gundiah N, Sane SP. Mechanics of the thorax in flies. J Exp Biol. 2017; 220 (8) 1382–1395. [PubMed: 28424311]

Dong S, Dong Y, Simões ML, Dimopoulos G. Mosquito transgenesis for malaria control. Trends Parasitol. 2022; 38 (1) 54–66. [PubMed: 34483052]

Duncan AB, Salazar BA, Garcia SR, Brandley NC. A sexual dimorphism in the spatial vision of north American band-winged grasshoppers. Integr Org Biology. 2021; 3 (1) obab008

Farkas R, Mechler BM. The timing of Drosophila salivary gland apoptosis displays an l(2)gl-dose response. Cell Death Differ. 2000; 7 (1) 89–101. [PubMed: 10713724]

Europe PMC Funders Author Manuscripts

Fernandes JJ, Keshishian H. Patterning the dorsal longitudinal flight muscles (DLM) of Drosophila: insights from the ablation of larval scaffolds. Development. 1996; 122 (12) 3755–3763. [PubMed: 9012497]

Fernandes J, Bate M, Vijayraghavan K. Development of the indirect flight muscles of Drosophila. Development. 1991a; 113 (1) 67–77. [PubMed: 1765009]

Fernandes J, VijayRaghavan K, Bate M. Development of the indirect flight muscles of Drosophila. 1991b; 77: 67–77.

Fernandes JJ, Celniker SE, VijayRaghavan K. Development of the indirect flight muscle attachment sites in Drosophila: role of the PS integrins and the stripe gene. Dev Biol. 1996; 176 (2) 166–184. [PubMed: 8660859]

Foster WA, Walker ED. Medical and veterinary entomology. Annu Rev Entomol. 2002; 32: 203–262.

Fu G, Lees RS, Nimmo D, Aw D, Jin L, Gray P, et al. Female-specific flightless phenotype for mosquito control. Proc Natl Acad Sci USA. 2010; 107 (10) 4550–4554. [PubMed: 20176967]

Grech K, Maung LA, Read AF. The effect of parental rearing conditions on offspring life history in Anopheles stephensi. Malar J. 2007; 6 (1) 130. [PubMed: 17892562]

Grimaldi D, Engel MS. Evolution Of The Insects. 2005. Available from: https://assets.cambridge.org/97805218/21490/frontmatter/9780521821490_frontmatter.pdf

Hall MJR, Martín-Vega D. Visualization of insect metamorphosis. Phil Trans Roy Soc Lond B Biol Sci. 2019; 374 (1783) 20190071 [PubMed: 31438819]

Harbarch, RE, Knight, KL. Taxonomists' Glossary of Mosquito Anatomy. Plexus Publishing Inc; 1980.

Hawkes FM, Dabiré RK, Sawadogo SP, Torr SJ, Gibson G. Exploiting Anopheles responses to thermal, odour and visual stimuli to improve surveillance and control of malaria. Sci Rep-uk. 2017; 7 (1) 17283

Hill SR, Ignell R. Modulation of odour-guided behaviour in mosquitoes. Cell Tissue Res. 2021; 383 (1) 195–206. [PubMed: 33486608]

Huijben S, Paaijmans KP. Putting evolution in elimination: winning our ongoing battle with evolving malaria mosquitoes and parasites. Evol Appl. 2018; 11 (4) 415–430. [PubMed: 29636796]

James AA, Rossignol PA. Mosquito salivary glands: parasitological and molecular aspects. Parasitol Today. 1991; 7 (10) 267–271. [PubMed: 15463385]

Jarvela AMC, Trelstad CS, Pick L. Regulatory gene function handoff allows essential gene loss in mosquitoes. Commun Biol. 2020; 3 (1) 540. [PubMed: 32999445]

Kawada H, Tatsuta H, Arikawa K, Takagi M. Comparative study on the relationship between photoperiodic host-seeking behavioral patterns and the eye parameters of mosquitoes. J Insect Physiol. 2006; 52 (1) 67–75. [PubMed: 16253268]

Keleta Y, Ramelow J, Cui L, Li J. Molecular interactions between parasite and mosquito during midgut invasion as targets to block malaria transmission. Npj Vaccines. 2021; 6 (1) 140. [PubMed: 34845210]

King JG, Hillyer JF. Spatial and temporal in vivo analysis of circulating and sessile immune cells in mosquitoes: hemocyte mitosis following infection. BMC Biol. 2013; 11 (1)

Lindstedt C, Murphy L, Mappes J. Antipredator strategies of pupae: how to avoid predation in an immobile life stage? Phil Trans Biol Sci. 2019; 374 (1783) 20190069

Louca V, Lucas MC, Green C, Majambere S, Fillinger U, Lindsay SW. Role of fish as predators of mosquito larvae on the floodplain of the Gambia river. J Med Entomol. 2009; 46 (3) 546–556. [PubMed: 19496426]

Malita A, Rewitz K. Interorgan communication in the control of metamorphosis. Curr Opin Insect Sci. 2021; 43: 54–62. [PubMed: 33214126]

Matthews BJ, Vosshall LB, Dickinson MH, Dow JAT. How to turn an organism into a model organism in 10 'easy' steps. J Exp Biol. 2020; 223 (Suppl. l_1) jeb218198 [PubMed: 32034051]

Medlock JM, Snow KR. Natural Predators and Parasites of British Mosquitoes –a Review, 1–11. European Mosquito Bulletin. 2008.

Meschi E, Ĺeopold P, Delanoue R. An EGF-responsive neural circuit couples insulin secretion with nutrition in Drosophila. Dev Cell. 2019; 48 (1) 76–86. e5 [PubMed: 30555002]

Metscher BD. MicroCT for comparative morphology: simple staining methods allow high-contrast 3D imaging of diverse non-mineralized animal tissues. BMC Physiol. 2009a; 9 (1) 11–14. [PubMed: 19545439]

Metscher BD. MicroCT for developmental biology: a versatile tool for high-contrast 3D imaging at histological resolutions. Dev Dynam. 2009b; 238 (3) 632–640.

Muijres FT, Chang SW, Veen WG, van Spitzen J, Biemans BT, Koehl MAR, et al. Escaping blood-fed malaria mosquitoes minimize tactile detection without compromising on take-off speed. J Exp Biol. 2017; 220 (20) 3751–3762. [PubMed: 29046418]

Nikbakhtzadeh MR, Buss GK, Leal WS. Toxic effect of blood feeding in male mosquitoes. Front Physiol. 2016; 7: 4. [PubMed: 26858651]

Niven JE, Graham CM, Burrows M. Diversity and evolution of the insect ventral nerve cord. Entomology (Tokyo). 2008; 53 (1) 253–271.

Niz MD, Kehrer J, Brancucci NMB, Moalli F, Reynaud EG, Stein JV, et al. 3D imaging of undissected optically cleared Anopheles stephensi mosquitoes and midguts infected with Plasmodium parasites. PLoS One. 2020; 15 (9) e0238134 [PubMed: 32936796]

Novak MG, Ribeiro JM, Hildebrand JG. 5-hydroxytryptamine in the salivary glands of adult female Aedes aegypti and its role in regulation of salivation. J Exp Biol. 1995; 198 (1) 167–174. [PubMed: 7891033]

Ogawa, Kichi; Kanda, T. Wingbeat frequencies of some anopheline mosquitoes of east asia(Diptera : Culicidae). Appl Entomol Zool. 1986; 21 (3) 430–435.

Organisation WH. World malaria report 2021. 2021. Available from: https://www.who.int/publications/i/item/9789240040496

Ramasamy R, Surendran SN. Mosquito vectors developing in atypical anthropogenic habitats: global overview of recent observations, mechanisms and impact on disease transmission. J Vector Dis. 2016; 53 (2) 91–98.

Ravichandran NK, Wijesinghe RE, Lee SY, Choi KS, Jeon M, Jung HY, et al. Non-destructive analysis of the internal anatomical structures of mosquito specimens using optical coherence tomography. Sensors Basel Switz. 2017; 17 (8) 1897.

Rishikesh N. Morphology and development of the salivary glands and their chromosomes in the larvae of ANOPHELES stephensi sensu stricto. Bull World Health Organ. 1959; 20 (1) 47–61. [PubMed: 13638789]

Rocha M, Kimler KJ, Leming MT, Hu X, Whaley MA, O'Tousa JE. Expression and light-triggered movement of rhodopsins in the larval visual system of mosquitoes. J Exp Biol. 2015; 218 (9) 1386–1392. [PubMed: 25750414]

Schoborg TA. Whole animal imaging of Drosophila melanogaster using microcomputed tomography. J Vis Exp. 2020; 163

Schoborg TA, Smith SL, Smith LN, Morris HD, Rusan NM. Microcomputed tomography as a platform for exploring Drosophila development. Development. 2019; 146 (23) dev176685 [PubMed: 31722883]

Seldin EB, White RH, Brown PK. Spectral sensitivity of larval mosquito ocelli. J Gen Physiol. 1972; 59 (4) 415–420. [PubMed: 5029552]

Snodgrass R. Smithsonian Miscellaneous Collections. The Anatomical Life of the Mosquito. 1959; 139: 1–93.

Surkova S, Görne J, Nuzhdin S, Samsonova M. Interplay between sex determination cascade and major signaling pathways during Drosophila eye development: perspectives for future research. Dev Biol. 2021; 476: 41–52. [PubMed: 33745943]

Thomas I. The reactions of mosquito larvae to regular repetitions of shadows as stimuli. Aust J Biol Sci. 1950; 3 (1) 113–123.

Tissot M, Stocker RF. Metamorphosis in Drosophila and other insects: the fate of neurons throughout the stages. Prog Neurobiol. 2000; 62 (1) 89–111. [PubMed: 10821983]

Tomé HV, Pascini TV, Dângelo RA, Guedes RN, Martins GF. Survival and swimming behavior of insecticide-exposed larvae and pupae of the yellow fever mosquito Aedes aegypti. Parasites Vectors. 2014; 7 (1) 195. [PubMed: 24761789]

Truman JW, Riddiford LM. The evolution of insect metamorphosis: a developmental and endocrine view. Phil Trans Roy Soc Lond B Biol Sci. 2019; 374 (1783) 20190070 [PubMed: 31438820]

VijayRaghavan K, Fernandes J, Bate M. Development of the indirect flight muscles of Drosophila. 1991; 77: 67–77.

White RH. Analysis of the development of the compound eye in the mosquito, Aedes aegypti. J Exp Zool. 1961; 148 (3) 223–239. [PubMed: 14006559]

Zirin J, Perrimon N, Cheng D, Dhanyasi N, Cho J, Dura J-Maurice, et al. Ecdysone signaling at metamorphosis triggers apoptosis of Drosophila abdominal muscles. Dev Biol. 2013; 383 (2) 275–284. DOI: 10.1016/j.ydbio.2013.08.029 [PubMed: 24051228]

Europe PMC Funders Author Manuscripts

Europe PMC Funders Author Manuscripts

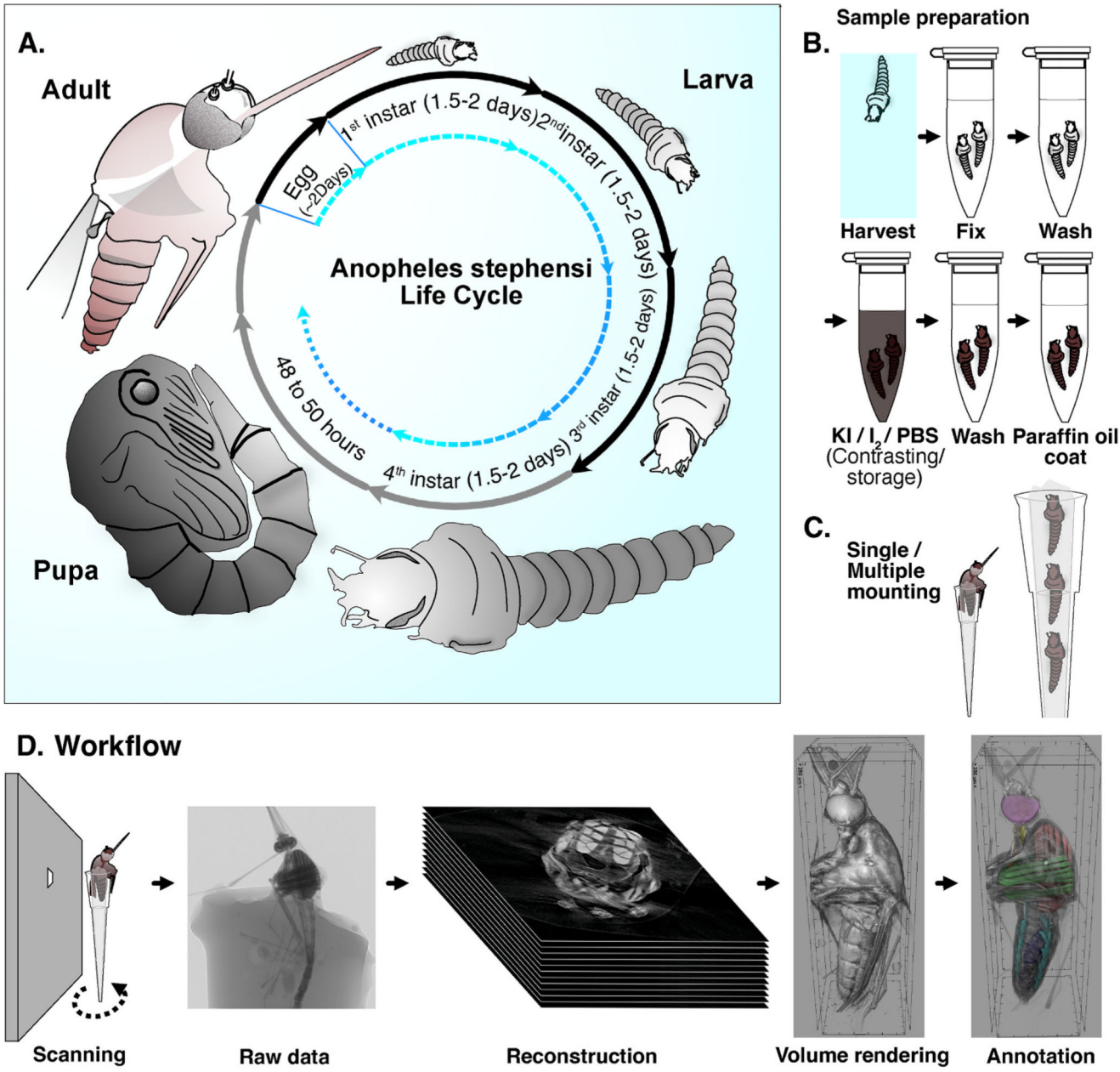

Fig. 1. *Anopheles stephensi* sample collection, scanning and analysis workflow

A. Schematic of *A. stephensi* life cycle under laboratory conditions. *A. stephensi* eggs hatch two days after oviposition and pass through four motile larval stages over a period of six to eight days to form pupae. Each pupa ecloses to give rise to adults in around 2 days. Pupae show reduced motility when compared to larvae. B. Samples to be scanned are collected at appropriate developmental stages and transferred to the fixing solution. Subsequently, samples are incubated in an aqueous iodine staining solution for standardized durations according to the developmental stage. Prior to scanning, samples are washed and coated with paraffin oil to prevent dehydration during scanning. C. Stained-oil-coated samples are positioned in petroleum jelly-filled polycarbonate micropipette tubes such that

the anterior-posterior axis is coaxial with the axis of the stage's rotation, as far as possible. D. Raw data consisting of X-Ray shadow images of samples are collected at appropriate rotation step sizes. These images are used to generate a 3D reconstruction stack of each scanned sample that can be annotated, segmented and volume-rendered as needed.

Europe PMC Funders Author Manuscripts

Europe PMC Funders Author Manuscripts

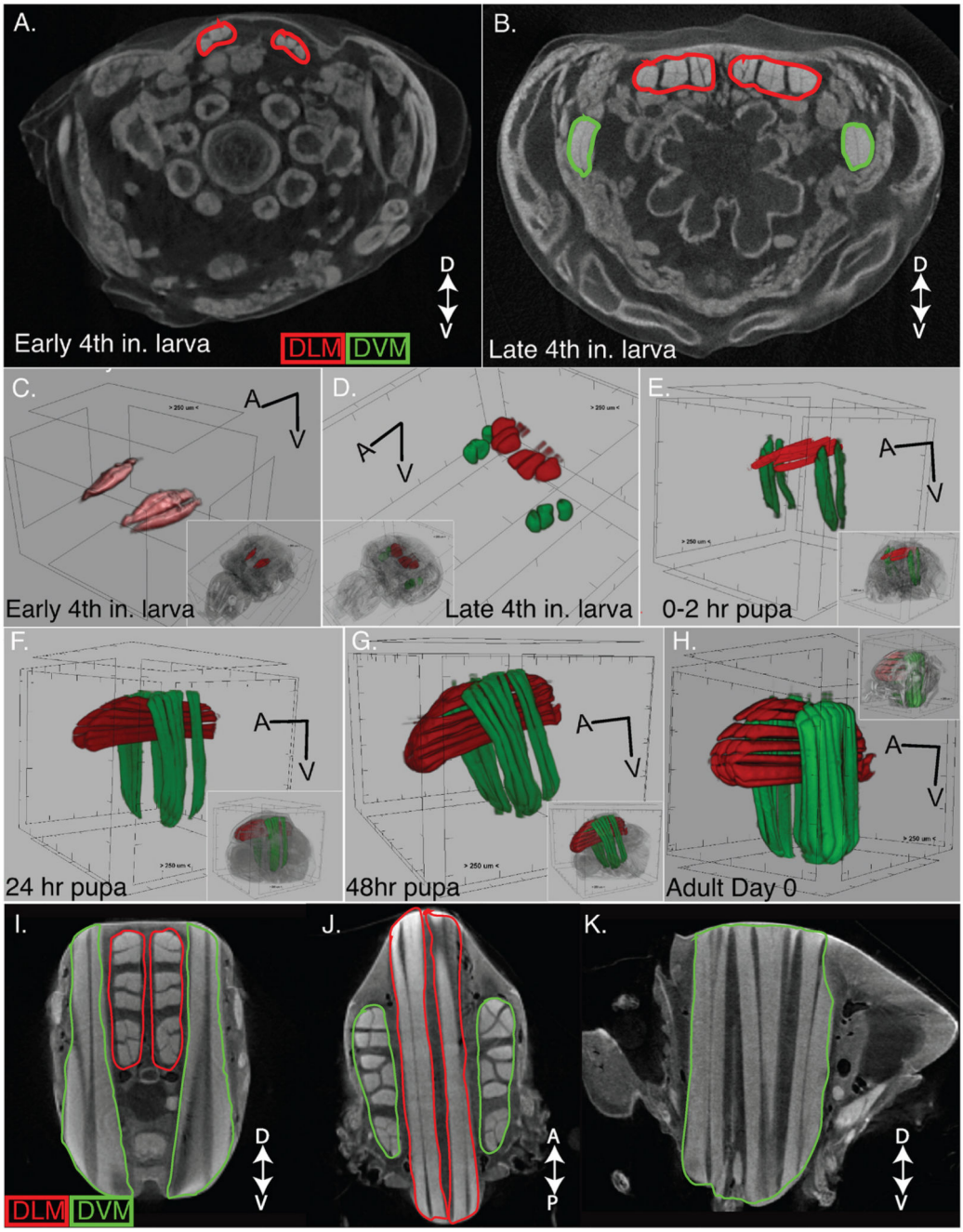

Fig. 2. *A. stephensi* Indirect Flight Muscle positioning and growth between 4th instar larval and adult stages.

Orientations: Anterior pointing towards the viewer out of the plane of reconstructed images (A., B., I.). Orientation arrows on each frame indicate a (anterior), p (Posterior), Dorsal (d) and v (Ventral). Indirect Flight Muscles: Dorsal Longitudinal Muscles (DLMs) outlined/colored in red, Dorso-Ventral Muscles (DVMs) outlined/colored in green in single pane views/3D reconstructions. Coronal views in reconstructed images through the thorax of 4th instar larvae (A-B). Structures outlined with a green dotted line (DVMs) in late 4th instar larvae (B.) are undetectable in early 4th instar larvae (A.). 3D rendering of indirect flight

muscles positioned in the thorax of larvae (C., D.), pupa (E.- G.), a day 0 adult (H.). Insets in panels (C.- H.) show the positioning of DLMs and DVMs within the whole thorax. I. Coronal view of reconstructed images of adults - In a day 5 adult thorax, 12 DLM fibers in three bundles of four are observed on either side of the sagittal mid-plane, DVMs positioned orthogonally on either side. J. Horizontal view of reconstructed images of adults - 12 DVM fibers in three bundles of four are observed on either side of DLMs. K. Dorso ventral muscle orientation (dorsal to ventral) relative to the anterior-posterior axis of reconstructed images of adults. Scalebar (A., B., I.-K.) = 100 μ; Separation between consecutive notches on bounding box = 250 μ (C.-H.).

Europe PMC Funders Author Manuscripts

Europe PMC Funders Author Manuscripts

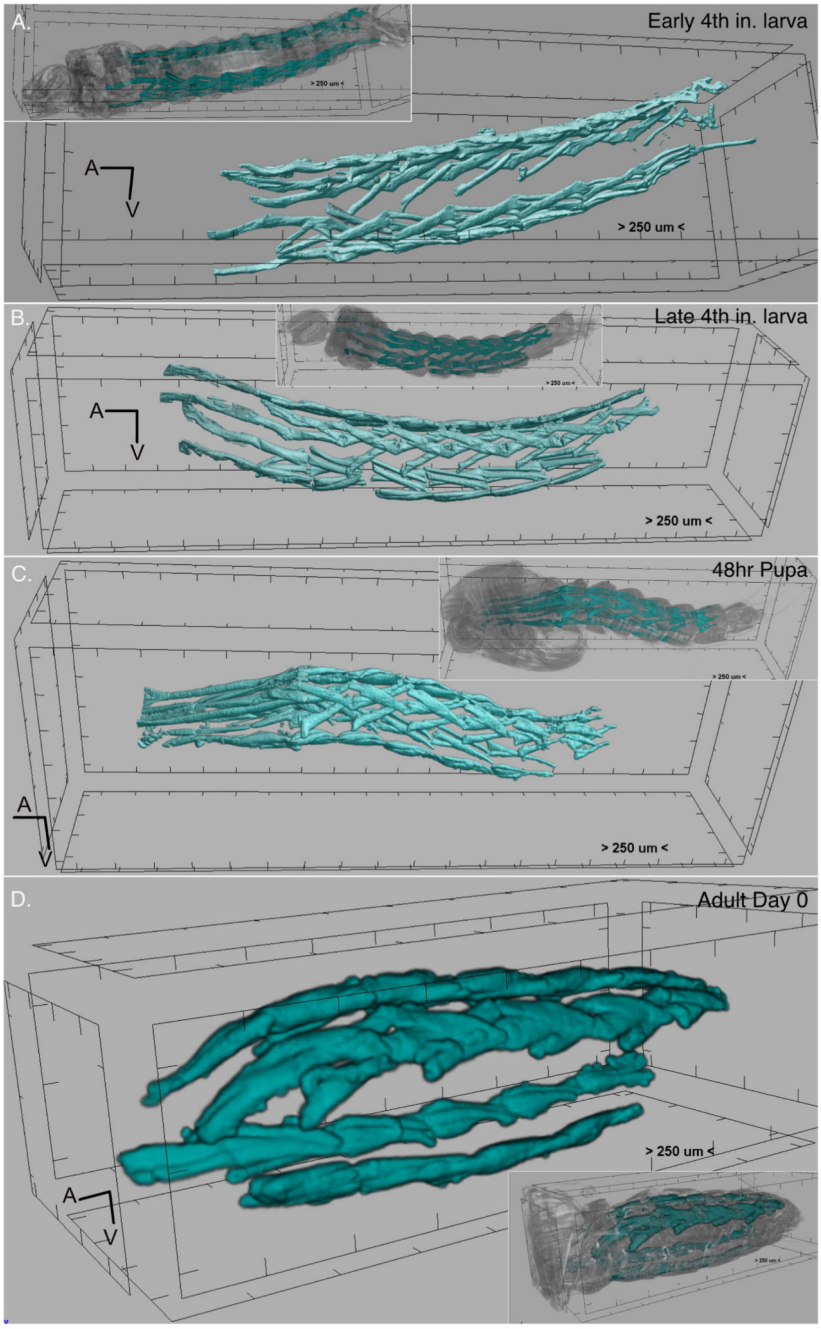

Fig. 3. *A. stephensi* Swim Muscle positioning and growth between 4th instar larval and adult stages.

3D rendering of swim muscles (sky blue) positioned within abdomens of a larva (A., B.), pupa (C.) and Day 0 post eclosion adult (D.) Insets show positioning within the whole animal. A and V indicate anterior and ventral directions. The separation between consecutive notches on bounding box = 250 μ.

Europe PMC Funders Author Manuscripts

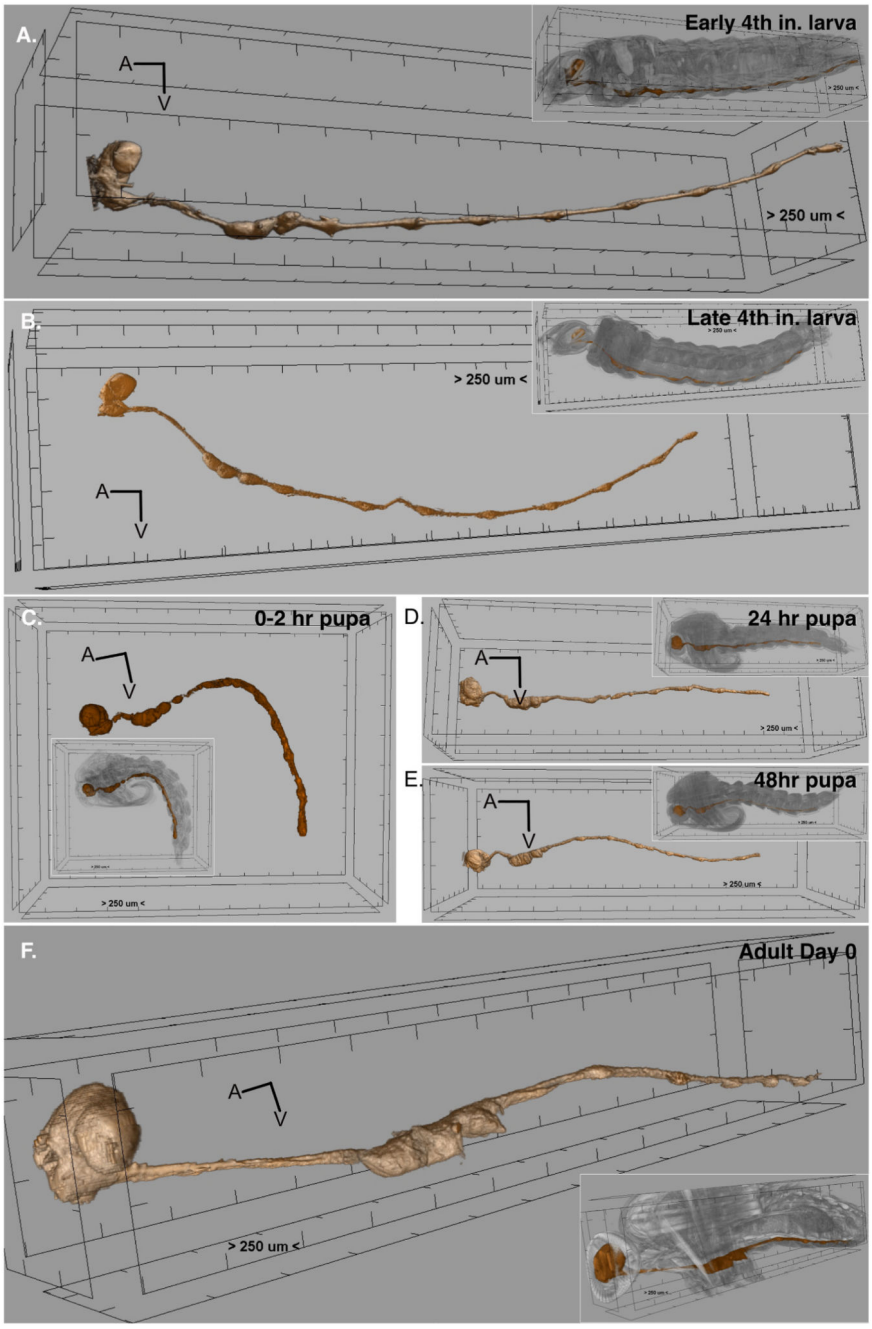

Fig. 4. *A. stephensi* Central Nervous System positioning between 4th instar larval and adult stages.

3D rendering of the nervous system (shades of brown), consisting of the brain, thoracic ganglia and abdominal ganglia positioned within whole bodies of a larva (A., B.), pupa (C.-E.) and Day 0 post eclosion adult (F.) Insets show positioning within the whole animal. In all panels, A and V indicate anterior and ventral directions. The separation between consecutive notches on the bounding box = 250 μ.

Europe PMC Funders Author Manuscripts

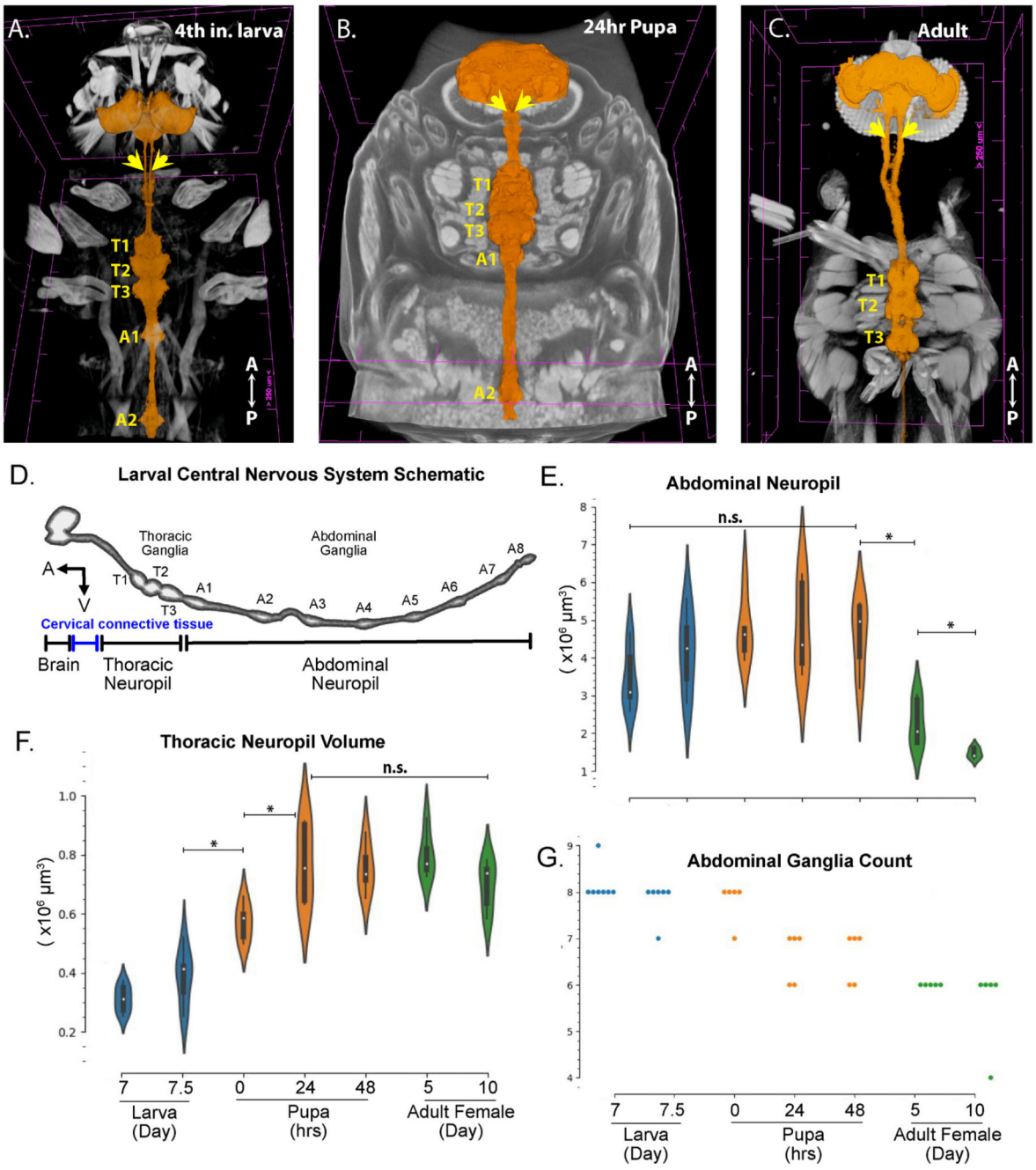

Fig. 5. *A. stephensi* Central Nervous System Development between 4th instar larval and adult stages.

Segmented brain, ventral nerve chord and thoracic ganglia depicted of 4th instar larva (A.), 24hr Pupa (B.) and Adult (C.): orange in the background of other tissue (grey), anterior pointing upwards in each frame. Yellow arrows indicate a bifurcated descending ventral nerve cord. T1, T2, T3 are numbered thoracic ganglia. A1, A2 and A3 are numbered abdominal ganglia. The separation between two consecutive notches: 250µ (D.) Schematic view of the larval nervous system. Pointers A and V mark the Anterior and Ventral sides of the animal. (E.) Violin plot depicting the volume of the abdominal component of the

CNS measured between larva day 7 and Adults. Two significant reductions in volume were seen between i) post-eclosion to day 5 adults, ii) day 5 adults to day 10 female adults. (F.) Violin plot depicting the volume of the thoracic components of the central nervous system measured between larva day 7 and adults. Two significant increases in volume were seen between i) 7.5 day larvae and 0hr pupae, ii) 0hr pupae and 24hr pupae. (n = 5 to 8 per time point) (G.) At least eight abdominal ganglia can be seen in day 7 larvae. Abdominal ganglia counts range from 8 to 6 in pupae and only 6 thereafter. *$p<0.05$, n.s. = not significant. n = 5 to 8 per time point.

Europe PMC Funders Author Manuscripts

Europe PMC Funders Author Manuscripts

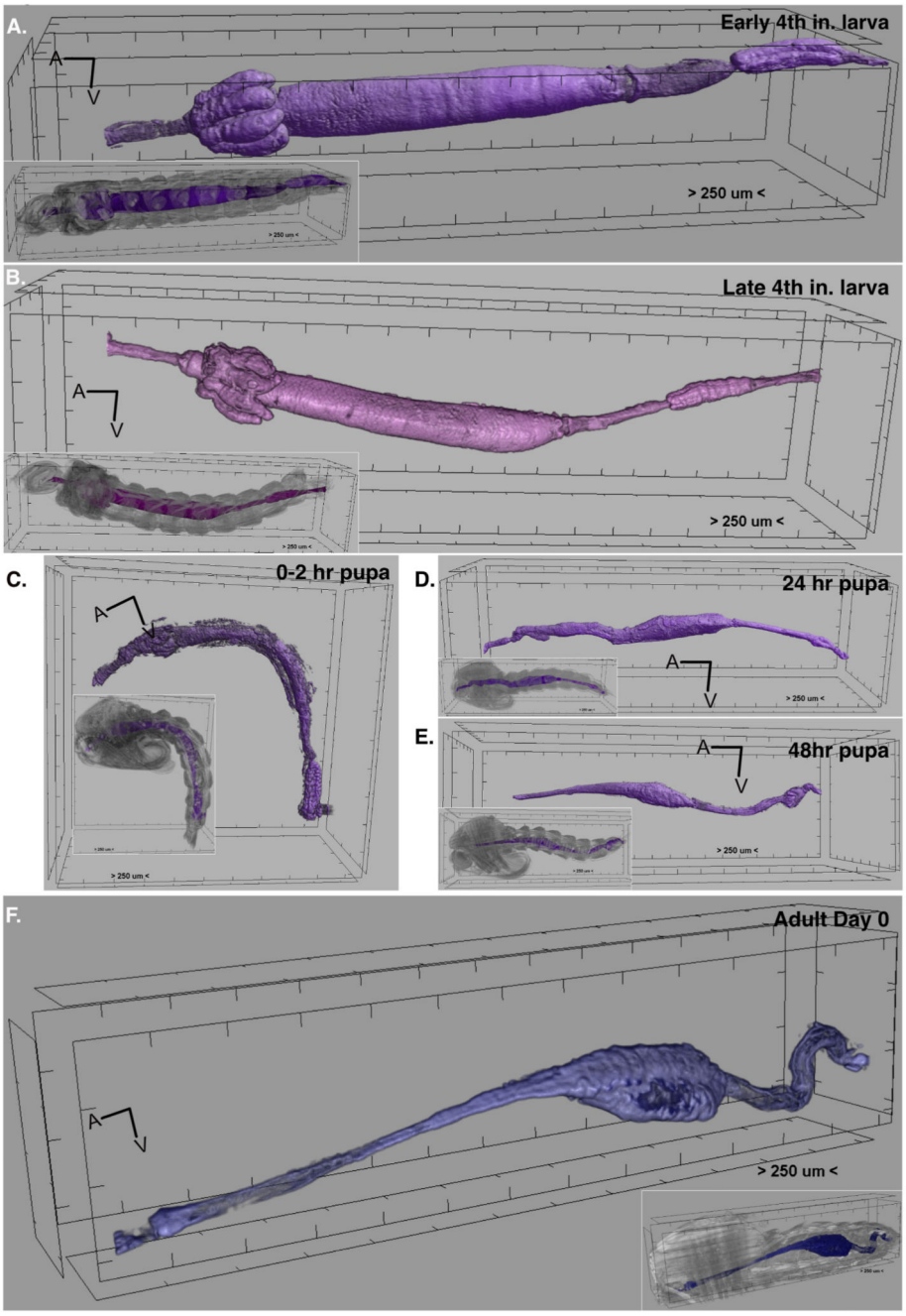

Fig. 6. *A. stephensi* alimentary canal positioning and growth between 4th instar larval and adult stages.

3D rendering of the alimentary canal (shades of purple), positioned within whole bodies of a larva (A., B.), pupa (C.- E.) and Day 0 post eclosion adult (F.) Insets show positioning within the whole animal. Gastric cecae (GC) are clearly seen extruding from the gastrointestinal tract within the larval thorax; Posterior to GC, the larval midgut extends to the 5th abdominal segment and narrows into the hindgut. (A. and B.). GC signals are obscured on the onset of pupariation (C.) and missing in late pupal stages (E.) In adults, the midgut is wide between the third and fourth abdominal segments. The current segmentation

protocol does not output malphigian tubules at the posterior end of the midgut. In all panels, A and V indicate anterior and ventral directions. The separation between consecutive notches on the bounding box = 250 μ.

Europe PMC Funders Author Manuscripts

Europe PMC Funders Author Manuscripts

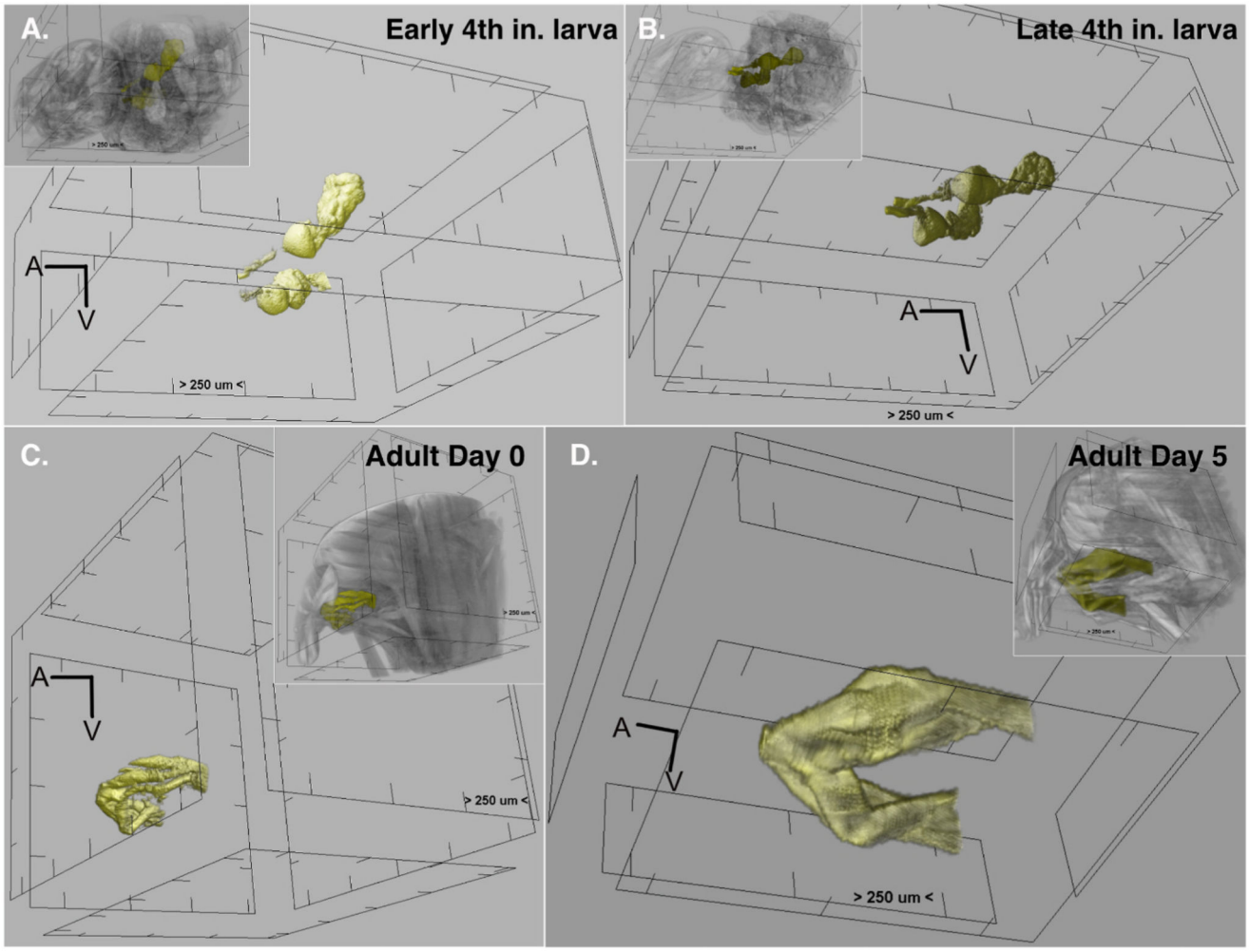

Fig. 7. *A. stephensi* Salivary Gland positioning between 4th instar larval and adult stages.

3D rendering of the Salivary gland (shades of yellow), positioned within whole bodies of a larva (A., B.), day 0 and day 5 post eclosion adults (C. and D.) No salivary gland structure can be discerned in pupae. Insets show positioning within the whole animal. In all panels, A and V indicate anterior and ventral directions. The separation between consecutive notches on the bounding box = 250 μ.

Europe PMC Funders Author Manuscripts

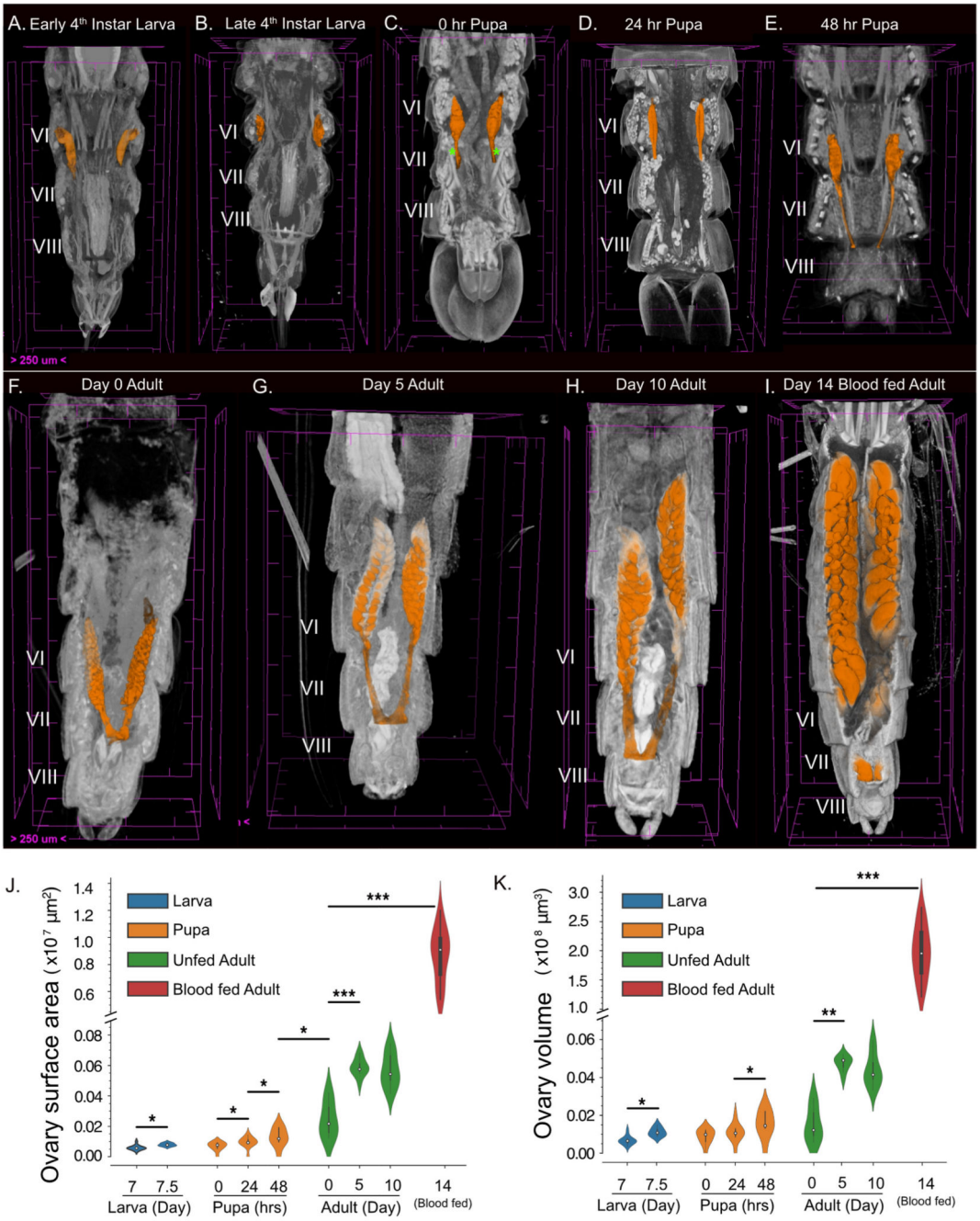

Fig. 8. *A. stephensi* ovary positioning and growth between 4th instar larval and adult stages.

3D renderings of the posterior abdomen with ovaries segmented in orange, of female Anopheline early 4th instar larvae(A, n = 14), late 4th instar larvae (B, n = 6), 0hr, 24 and 48 h pupae (C-E, n = 10 each), unfed adults at 0, 5 and 10 days post eclosion (F-H, n = 6,10,10 respectively) and a 14 day old female blood fed at 5 days post eclosion (I, n = 18). Roman numerals indicate the abdominal body segment number. Green asterisks indicate first segmentable appearance of lateral oviducts (C). Ovary surface areas (J) and volumes

(K) violin plotted with each developmental stage with indicated color code. The separation between consecutive notches on the bounding boxes = 250 μ.

Europe PMC Funders Author Manuscripts

Europe PMC Funders Author Manuscripts

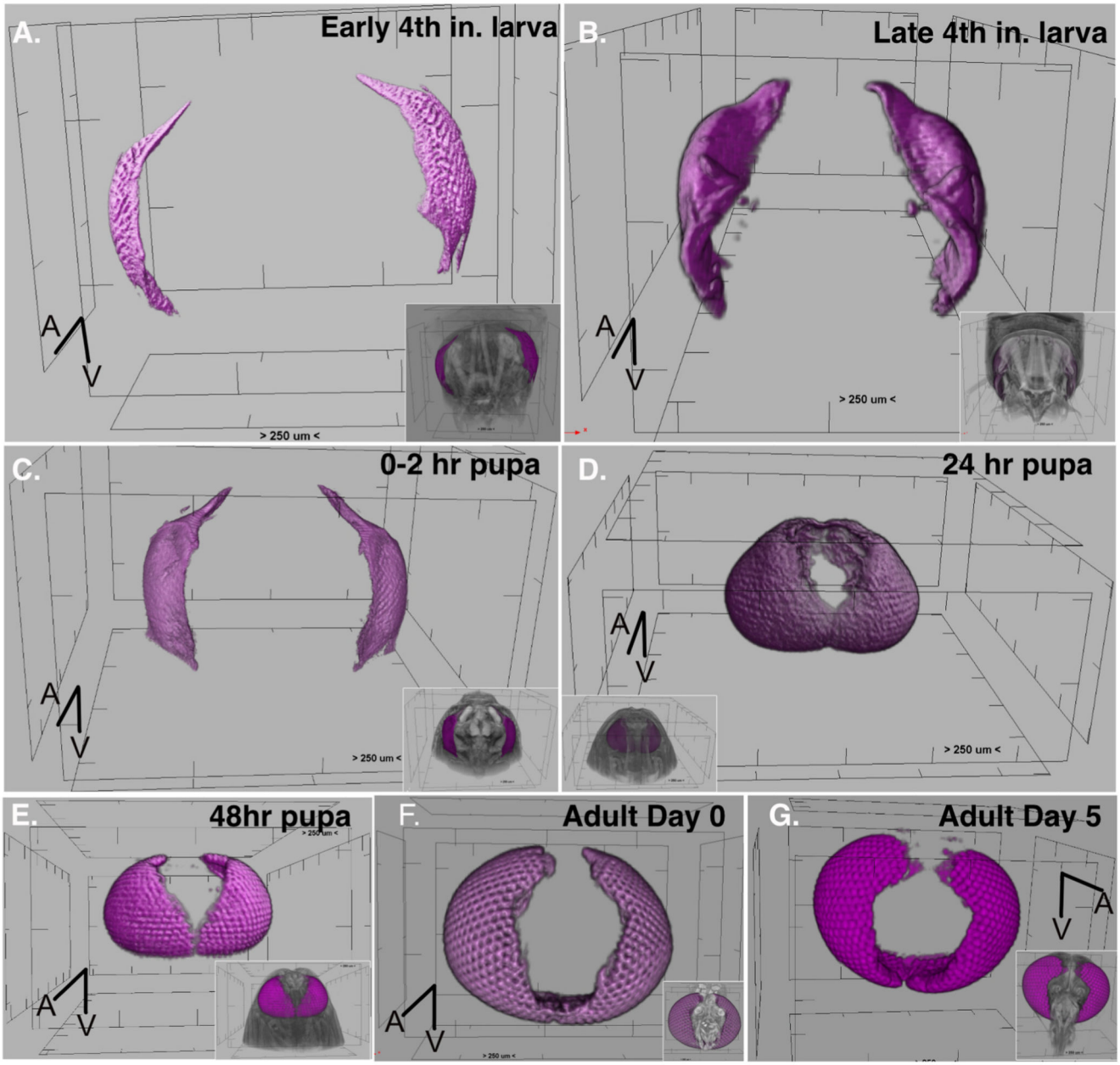

Fig. 9. *A. stephensi* eye positioning and growth between 4th instar larval and adult stages.

3D rendering of the eyes (shades of magenta), positioned on whole heads of a larva (A., B.), pupa (C. to E.), adult day 0 and day 5 post eclosion adults (F. and G.). Two distinct fields of facets comprising compound eyes can be seen on either side of the head from early larval stages to until early pupae (A.- C.). Thereafter the two separate fields of eye facets meet at the ventral side of the head, posterior to mouthparts. Insets show eye positioning on the head of each animal. In all panels, A and V indicate anterior and ventral directions. The separation between consecutive notches on the bounding box = 250 μ.

Europe PMC Funders Author Manuscripts

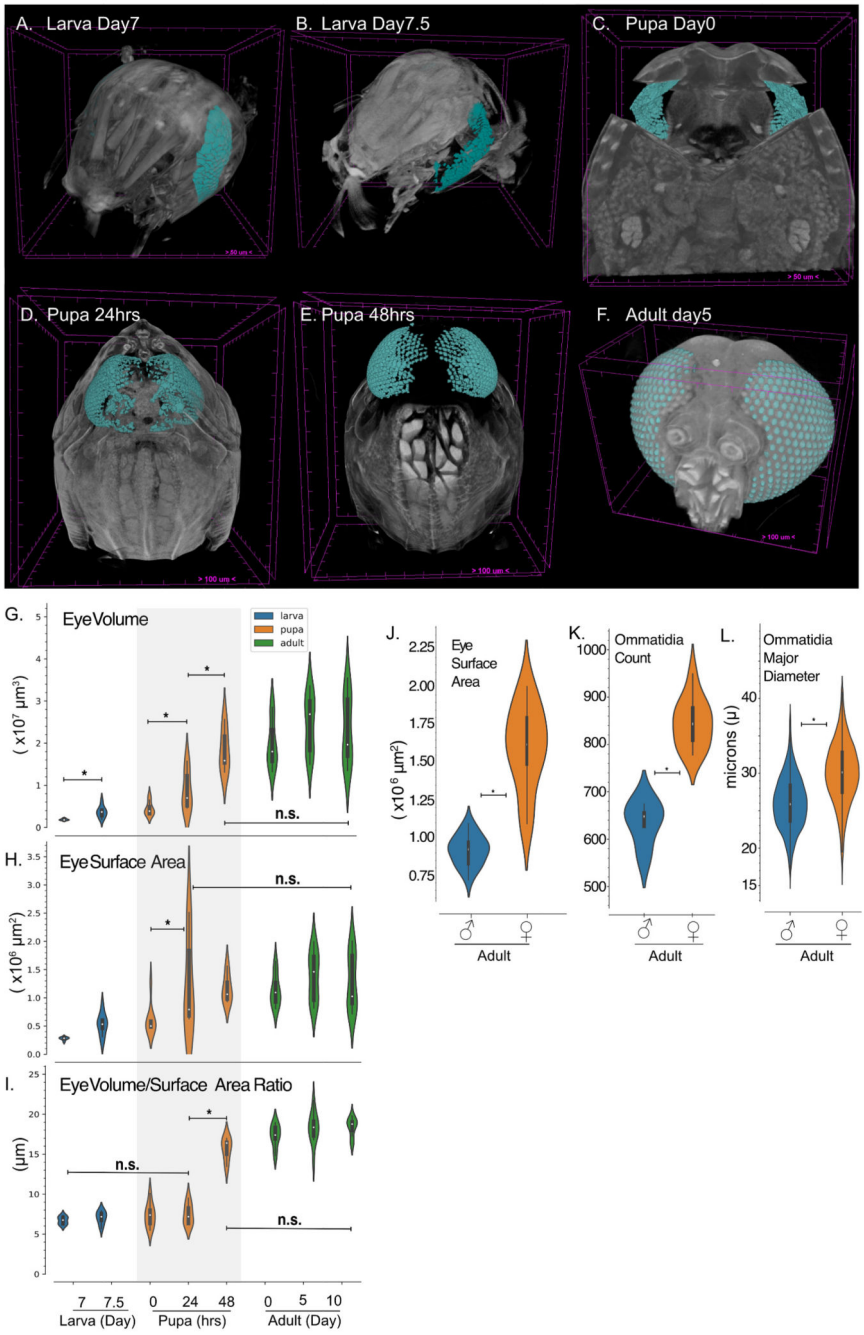

Fig. 10. *A. stephensi* eye and ommatidia measurements between 4th instar larval and adult stages.

Segmented ommatidia (cyan) within eyes as seen in larvae to adults (A.) to (F.) based on size and shape. Anterior points to the bottom left of A., B., F. and towards the viewer in C., D., E. Scale as noted on each panel. Violin plots depict measurements in both eyes pooled from male and female animals at specified developmental stages (G.) The total volume of ommatidia. (H.) The total surface area of eyes (n = 15 to 18), (I.) Eye volume to surface area ratio from individual animals (n = 5 to 12 at all stages). Violin plots comparing males and females 0, 5 and 10 day p.e. eyes (J.) total surface area (K.) Ommatidia count (L.)

Distribution of the major diameter of ommatidia (in microns) in eyes compared between. (n = 4 males, 12 females).

Europe PMC Funders Author Manuscripts